Vibration Control for Electric Vehicle with In-Wheel Motors on Slippery Road using Driving Force Control

Tomonori Suzuki* Student Member,
Yoichi Hori* Fellow,
Etsuo Katsuyama** Non-member
Hiroshi Fujimoto* Senior Member
Naoto Shimoya** Non-member

For the purpose of the vehicle ride comfort improvement, a number of studies on vibration suppression control have been conducted. The ride comfort can be enhanced more by precise traction force control in electric vehicles because of their higher motion performance than that in internal combustion engine vehicles. However, conventional vibration suppression control methods are not able to exhibit their performance sufficiently on slippery roads, because conventional studies lack the consideration of wheel slip. In this paper, we propose a vibration suppression control method with driving force control to achieve the high robustness against the road condition variations. The effectiveness of the proposed method is evaluated by simulations and experiments in an in-wheel motor vehicle.

Keywords: Vibration control, Vehicle motion control, Electric vehicle, In-wheel motor, Low μ road, Driving force control.

1. Introduction

In recent years, electric vehicles (EVs) are attracting a lot of attention due to increasing environmental awareness. In addition, EVs have higher motion performance than internal combustion engine vehicles because of their motor characteristics. Motors have three major advantages over internal combustion engines: torque response is several hundred times faster and more accurate than that in the internal combustion engine, output torque can be directly measured from the motor current value, it is possible to distribute motors for flexible arrangement [1]. By utilizing these features effectively, advanced vehicle motion control becomes possible [2][3].

In particular, distributed arrangement of motors enables various drivetrain configurations in EVs. One of them is an in-wheel motor (IWM) system in which the motors are mounted in each wheel. The IWM system has the advantages of reducing the total weight of a drivetrain and increasing freedom of indoor layout designing [4]. From a control perspective, torque vectoring enables higher motion performance and the shorter drive shaft removes low-frequency resonances which is a strong limitation in current control structures [5][6].

In order to improve motion performance and ride comfort, several vibration suppression control methods which lie in the several Hz bands have been proposed [7][8]. However, the IWM system increases the unsprung weight, and it causes deterioration of ride comfort over 4 Hz. In order to solve this problem, advanced studies on vibration suppression for the unsprung vertical axis mode and the longitudinal axis mode that lay in a higher frequency band (10 Hz and above) have been conducted [9][10].

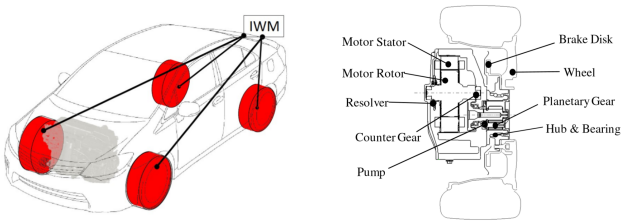

(a) Experimental vehicle. (b) IWM unit.

Fig. 1. Experimental vehicle with IWM units.

These vibration suppression controls in the high frequency use high torque response of the IWM system. As described above, widespread research using the IWM system has been carried out to suppress vibration in wide frequency.

However, the conventional vibration suppression control using the IWM system cannot be applied in wheel slip condition such as on the slippery road with low friction coefficient μ (low μ road), since these conventional methods are not capable of controlling driving force when a wheel slips. Meanwhile, our research group has proposed a driving force control method that can prevent slipping and directly control the driving force [11]. This method has been developed with the aim of the driving force proper control on any road surface condition.

In this paper, we combined the driving force control with the triple skyhook control (tSH) [7] which is a vertical vibration suppression control method. The effectiveness of the proposed method is evaluated on the low μ road where a wheel slips easily. Our group conducted simulations and experiments and validated the effectiveness of the proposed method.

* The University of Tokyo
5–1–5, Kashiwanoha, Kashiwa, Chiba, 277–8561, Japan
** Toyota Motor Corporation
1200, Mishuku, Susono, Shizuoka, 410–1193, Japan

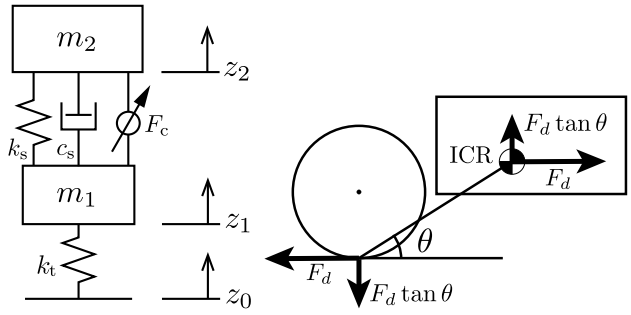

(a) Quarter car model. (b) Suspension reation force model.

Fig. 2. Vehicle Model.

Table 1. Vehicle model parameters definition.

Symbol	Meaning	Symbol	Meaning
m_1	Unsprung mass	m_2	Sprung mass
k_s	Spring stiffness	c_s	Damping coefficient
k_t	Tire stiffness	z_0	Displacement of road
z_1	Displacement of unsprung mass	z_2	Displacement of sprung mass
J	Equivalent inertia of wheel	V_ω	Wheel velocity
V	Vehicle velocity	T	Motor torque
F_d	Driving force	r	Tire raduis
N	Normal force of tire	μ	Friction coefficient
D	Driving stiffness	F_c	Suspension reaction force

2. Experimental vehicle and vehicle model.

2.1 Experimental IWM vehicle The vehicle shown in Fig. 1(a) is used as an experimental vehicle. The vehicle has four IWM units shown in Fig. 1(b), and this vehicle is equipped with four vertical acceleration sensors on the sprung mass.

2.2 Vehicle vibration model The quarter car model is shown in Fig. 2(a). The definition of each variable is indicated in Table 1. F_c is suspension reaction force which is described later. The dynamic equations for the quarter car model are given as follows:

$$m_2\ddot{z}_2 = k_s(z_1 - z_2) + c_s(\dot{z}_1 - \dot{z}_2) + F_c, \quad (1)$$

$$m_1\ddot{z}_1 = -k_s(z_1 - z_2) - c_s(\dot{z}_1 - \dot{z}_2) + k_t(z_0 - z_1) - F_c. \quad (2)$$

2.3 Suspension reaction force The suspension reaction force is a component of the driving force acting in the vertical direction between the sprung and unsprung mass via the suspension arm.

Fig. 2(b) shows the front wheel model. The arm between the sprung and unsprung mass has a structure that rotates around the instant center of rotation (ICR). The driving force in the longitudinal direction working on the tire causes a moment to the arm. Then, the vertical force that balances the moment of the driving force is generated.

Assuming that the angle between the ground and ICR of the arm is θ and the magnitude of the driving force is given as F_d, the suspension reaction force in the vertical direction F_c can be calculated as follows:

$$F_c = F_d \tan\theta. \quad (3)$$

2.4 Vehicle motion and tire model If the running resistance is sufficiently small and a wheel axle is rigid, the motion equations of the wheel and the vehihcle can be expressed as follows:

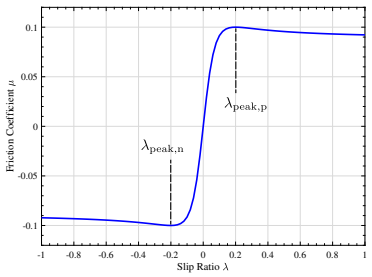

Fig. 3. $\mu - \lambda$ characteristics.

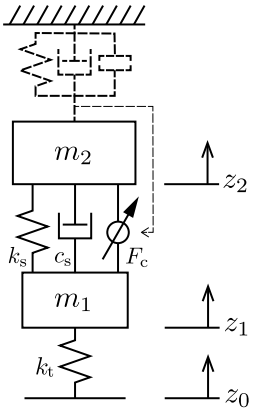

Fig. 4. Triple skyhook control concept.

$$J\frac{\dot{V}_\omega}{r} = T - rF_d, \quad (4)$$

$$(m_1 + m_2)\dot{V} = F_d, \quad (5)$$

where the definition of each variable is indicated in Table 1. For ease of description, we assumed reduction gear ratio of the motor is 1.

During driving or braking, the wheel velocity $V_\omega = r\omega$ is not equal to the vehicle velocity V due to the elastic deformation of the tire.

At this time, the slip ratio λ is defined for this difference as follows:

$$\lambda = \frac{V_\omega - V}{\max(V_\omega, V, \epsilon)}. \quad (6)$$

ϵ is a small constant to prevent division by zero.

The driving force F_d generated in each wheel is expressed by the equation (7) using the normal force N and the friction coefficient μ. Moreover, the driving stiffness D is defined as shown in (8).

$$F_d = \mu N \quad (7)$$

$$D = \frac{dF_d}{d\lambda} \quad (8)$$

Here, the relation between the slip ratio λ defined in (6) and the friction coefficient μ is as shown in Fig. 3.

According to Fig. 3, there are slip ratios $\lambda_{peak,p}$ and $\lambda_{peak,n}$ where μ takes the maximum and minimum value. The tire is in the adhesion state when $\lambda_{peak,n} \le \lambda \le \lambda_{peak,p}$, and the tire generates a dynamic friction force out of this adhesion region. In this adhesion region, the relation between μ and λ can be linearly approximated, and the driving stiffness D becomes constant as follows:

$$D|_{\lambda_{peak,n} \le \lambda \le \lambda_{peak,p}} = \frac{\mu}{\lambda}N. \quad (9)$$

Suppressing the slip ratio within this adhesion region at all times enables driving stiffness to be constant and the driving force is proportional to the slip ratio λ.

3. Vibration suppression control on low μ road

3.1 Proposed combination method Our research group expects that the combination of the vibration suppression control method and the driving force control method improves vibration suppression performance on the low μ road

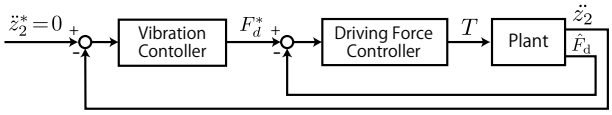

Fig. 5. Block diagram of the proposed method.

as well as on the high μ road. Driving force control suppresses wheel slip and control driving force even on the low μ road.

The block diagram of the proposed method is shown in Fig. 5. In this paper, the triple skyhook control [7] is used for vertical vibration suppression control. The triple skyhook controller determines the driving force command value with respect to the sprung vertical acceleration. Then the driving force controller controls the driving force.

3.2 Triple skyhook control This control feeds back the vertical displacement, velocity, and acceleration of the sprung mass.

The control input is expressed as follows:

$$F_c = -\alpha(m_2 s^2 + c_s s + k_s) z_2, \tag{10}$$

where α is a control gain.

This means that the sprung mass is hooked with virtual three elements: spring, damper, and inerter as shown in Fig. 4. As a result, z_2 is multiplied by $1/(1+\alpha)$ compared to without control.

3.3 Driving force control The block diagram of the driving force control is shown in Fig. 6. The outer loop is a driving force loop, and the inner loop is a wheel velocity loop works as the slip ratio control. F_d^* is a driving force command value, and $\hat{F}_d$ is the driving force estimated by the driving force observer [11].

The slip ratio is defined as shown in (6). However this is inconvenient for control because the definition of the slip ratio is different in driving ($V_\omega \geq V$) and in braking ($V_\omega < V$). Therefore, instead of the slip ratio defined in (6), the manipulated variable y defined by the following equation is used.

$$y = \frac{V_\omega}{V} - 1 \tag{11}$$

This is the same definition as the slip ratio in braking. The relationship between λ and y in driving can be given as (12).

$$y = \frac{\lambda}{1-\lambda} \tag{12}$$

Therefore, even in driving, y and λ are nearly equal around $\lambda = 0$.

From (11), the command value V_ω^* for wheel velocity control is expressed by the following equation.

$$V_\omega^* = (1 + y^*)V \tag{13}$$

However, in this definition, V_ω^* becomes 0 as long as $V = 0$ and the vehicle cannot start moving. Therefore, we change the command value as follows:

$$V_\omega^* = V + \max(V, \sigma) y^*, \tag{14}$$

where σ is a small constant.

As mentioned in (8) and (9), driving force is approximately represented as $F_d = D\lambda$ using the constant D when λ is sufficiently small. Furthermore, if the wheel velocity control of the inner loop is sufficiently fast and $y \simeq \lambda$ always holds true, the transfer function from y to F_d is represented by the zeroth order as follows:

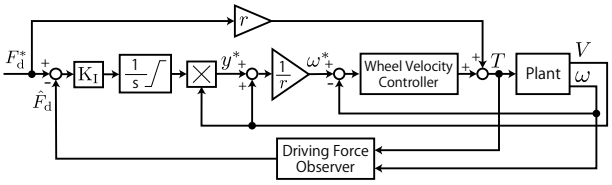

Fig. 6. Block diagram of driving force control.

$$F_d = D\lambda \simeq Dy. \tag{15}$$

Then we use an I controller as the driving force controller.

By setting the upper limit y_{max} and lower limit y_{min} to the integrator of the driving force controller and limiting y^* to $y_{min} < y^* < y_{max}$, the slip ratio can be controlled in the linear region.

4. Simulation

The simulation was conducted in order to evaluate the vibration suppression effect of the proposed method. The proposed method is compared with the triple skyhook control without the driving force control and the method without any vibration suppression control.

The sprung mass acceleration $\ddot{z}_2$ was simulated on the following condition. A sine wave road displacement disturbance, the amplitude is 0.02 m and the frequency is 1.5 Hz, is input to the vehicle model. The road surface friction coefficient μ is set 0.1. The initial velocity of the vehicle is 27 km/h, and −1000 N is added to the driving force command value in order to realize a situation where common drivers brake.

The controller is set as below. The pole of the wheel velocity controller in the driving force controller is designed to be 0.2 Hz. I gain of the driving force controller is 0.001 and the bandwidth of the driving force observer is 12 Hz. The lower and upper limits of the slip ratio command values are $y_{min} = -0.2$ and $y_{max} = 0.25$. The triple skyhook controller gain α is 1.4.

Simulation results are shown in Fig. 7. As shown in Fig. 7(a), the proposed method shows the best vibration suppression effect. The root mean square (RMS) of the sprung mass accelerations of each conditions are 2.66, 3.66, and 3.86 m/s^2 respectively. The differences of the vibration suppression effects are caused by the wheel slip as shown in Fig. 7(b). The proposed method successfully suppresses the slip ratio within the adhesion region of a tire. In contrast, the vibration suppression controller without the driving force control increases slip ratio, and it makes the driving force uncontrollable.

5. Experiment

The effectiveness of the proposed method was verified by the vehicle test.

The condition of the experiment is equal to the simulation but only the disurbance is different. In the experiment, a disturbance is intentionally generated by the motor for reproducibility. A sine wave with an amplitude of 1200 N and 1.5 Hz is added to the driving force command value.

The vibration suppression and disturbance controls were

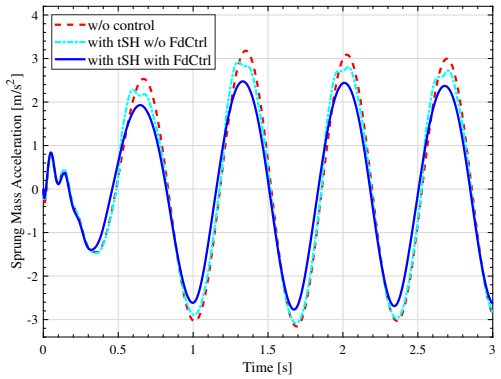

(a) Comparison of the sprung mass acceleration of each control method.

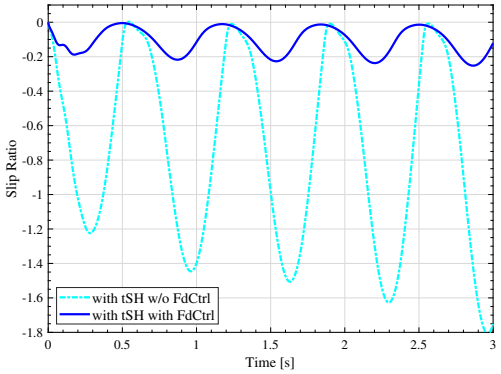

(b) Comparison of the slip ratio of each control method.

Fig. 7. Simulation result on the low μ road.

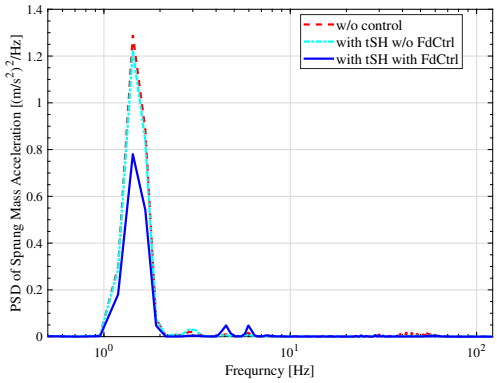

(a) Comparison of PSD of the sprung mass acceleration of each control method.

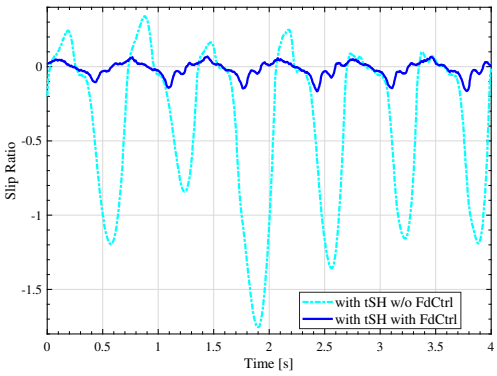

(b) Comparison of the slip ratio of each control method.

Fig. 8. Experiment result on the low μ road.

implemented in the rear wheels. The vehicle velocity is obtained from the wheel velocity of the front non-driven wheel.

The experimental result is shown in Fig. 8. As shown in Fig. 8(a), power spectrum density (PSD) of the rear sprung mass vertical acceleration in the proposed method is greatly suppressed as compared to other methods. The values of PSD at 1.5 Hz are 0.78, 1.22 and 1.29 respectively. The proposed method improves vibration suppression performance by 36 % than only the triple skyhook control. Moreover, as shown in Fig. 8(b), the slip ratio of the proposed method was suppressed within the adhesion region of the tire. On the other hand, the slip ratio of only the triple skyhook control changes largely.

6. Conclusion

This paper proposed the combination method of the triple skyhook control and the driving force control in order to suppress the vibration even on the low μ road. The driving force control method generates an accurate driving force in the adhesion region. Even for the driving force command value exceeding the physical limit, the driving force control keeps the slip ratio in the adhesion region and suppresses the slip. Therefore, the proposed method suppresses the vibration even on the low μ road. The simulations and experiments clarified that the proposed method has larger vibration suppression effect than the conventional method on the low μ road.

Acknowledgment

This work was partly supported by JSPS KAKENHI Grant Number 18H03768.

References

(1) Y. Hori, "Future Vehicle Driven by Electricity and Control-Research on Four-Wheel-Motored "UOT Electric March II"," *IEEE Transactions on Industrial Electronics*, vol. 51, no. 5, pp. 954–962, 2004.

(2) V.-D. Doan, H. Fujimoto, T. Koseki, T. Yasuda, H. Kishi, and T. Fujita, "Iterative Dynamic Programming for Optimal Control Problem with Isoperimetric Constraint and Its Application to Optimal Eco-driving Control of Electric Vehicle," *IEEJ Journal of Industry Applications*, vol. 7, no. 1, pp. 80–92, 2018.

(3) T. Ohhira and A. Shimada, "Movement Control Based on Model Predictive Control with Disturbance Suppression using Kalman Filter including Disturbance Estimation," *IEEJ Journal of Industry Applications*, vol. 7, no. 5, pp. 387–395, 2018.

(4) S. Murata, "Innovation by in-wheel-motor drive unit," *Vehicle System Dynamics*, vol. 50, no. 6, pp. 807–830, 2012.

(5) V. Ivanov, D. Savitski, J. Orus, J. M. R. Fortun, A. Sorniotti, and P. Gruber, "All-wheel-drive electric vehicle with on-board motors: Experimental validation of the motion control systems," *IECON 2015 - 41st Annual Conference of the IEEE Industrial Electronics Society*, pp. 1729–1734, 2015.

(6) J. M. Rodriguez, R. Meneses, and J. Orus, "Active vibration control for electric vehicle compliant drivetrains," *IECON 2013 - 39th Annual Conference of the IEEE Industrial Electronics Society*, pp. 2590–2595, 2013.

(7) E. Katsuyama, "Improvement of ride comfort by triple skyhook control," in *9th International Munich Chassis Symposium 2018*, 2018, pp. 215–234.

(8) N. Ochi, H. Fujimoto, and Y. Hori, "Proposal of roll angle control method using positive and negative anti-dive force for electric vehicle with four in-wheel motors," *2013 IEEE International Conference on Mechatronics, ICM 2013*, pp. 816–821, 2013.

(9) E. Katsuyama and A. Omae, "Improvement of Ride Comfort by Unsprung Negative Skyhook Damper Control Using In-Wheel Motors," *SAE International Journal of Alternative Powertrains*, vol. 5, no. 1, pp. 2016–01–1678, 2016.

(10) S. Ohno and K. Ito, "Unsprung vibration control for in-wheel-motor EV," *JSAE Autumn Congress 2014*, no. 103, pp. 21–24, 2014.

(11) H. Fujimoto, M. Yoshimura, and M. Formula, "Driving Force Control for Electric Vehicle Based on Slip Ratio Control," *JSAE Spring Congress 2011*, vol. 20, no. 20115112, pp. 8–11, 2011 (in Japanese).